Study on increasing approval and acceptance of AI systems for clinical use of machine learning to using xAI to detect Heat Stroke

Tashin Chowdhury[1], Hafiz Al Asad[1], Adiba Sharif [1], Md. Shamsur Rahman Khan[1], Mohammad Monirujjaman Khan[1]

[1]Department of Electrical and Computer Engineering, North South University, Bashundhara, Dhaka-1229, Bangladesh

[*]Corresponding Author: Mohammad Monirujjaman Khan

Email: monirujjaman.khan@northsouth.edu

Abstract: The most deadly ailment caused by excessive heat is heat stroke. The body's temperature rises quickly, the sweating mechanism malfunctions, and the body is unable to cool down. It happens when the body can no longer regulate its temperature. The body temperature can increase to 106°F or more within 10 to 15 minutes of a heat stroke. If the sufferer does not receive emergency care, heat stroke can result in lasting impairment or death. The Indian subcontinent saw an extended period of high heat in April, May, and June of 2015, which contributed to more than 2,500 deaths in India and more than 1,100 deaths in Pakistan. India's meteorological agency announces a heat wave when the air temperature at the surface exceeds the average daily maximum temperature. Heat waves are widespread in India between March and June[2]. Heatwaves, or extremely hot weather that might linger for many days, can have a serious negative effect on civilization, including an increase in fatalities from exposure to the sun. Heat waves are among the most destructive natural disasters, but because their death tolls and destruction are not usually evident, they rarely receive appropriate attention. Over 166 000 people died as a result of heatwaves from 1998 to 2017, including over 70 000 individuals who perished in Europe during the 2003 heatwave. Symptoms of heat stroke include confusion, altered mental status, slurred speech, unconsciousness, hot, dry skin or excessive sweating, convulsions, extremely high body temperature, and lethal if treatment is postponed. A lot of work has been done on using machine learning to predict heatstrokes in patients. What sets our work standing is the use of xAI to increase approval and acceptance of AI in the use of pathology.

Keywords: Heat Stroke; xAI, CNN; Python; tabular dataset; data augmentation; MobileNetV2; ResNet50; VGG16; transfer learning.

1 Introduction

The current heatstroke statistics is very lamentable because the hottest days of summer seems to be growing more warmer than the recorded hottest day from the previous summers. On the July of 2022, 70 people in Bangladesh lost their lives to three different types of heat related causes. The EU is vulnerable too as they have not recuperated from the first wave. On 26 April 2021, the total number of infected people in India was 360,960, which is increasing rapidly [1]. This is distressing for Bangladesh because of the close geographical location between these countries, and the Indian variant of SARS-CoV-2 is more dangerous than the other variants. The virus is spreading very fast and can be contracted at all ages, which can lead to serious illness. As a highly contagious viral disease caused by SARS-CoV-2, COVID-19 has wreaked havoc on the world's demography, killing over 2.9 million people globally, making it the most significant global health epidemic since the 1918 influenza pandemic. Patients older than 60 years, as well as those with medical problems, should be considered at a higher risk of being infected by SARS-CoV-2 [2]. According

to the estimates of the World Health Organization, there are approximately 167,011,807 COVID-19 cases worldwide [3 Heatstroke is a potentially fatal condition caused by your body overheating. It's characterized as having a body temperature more than 104 degrees Fahrenheit (40 degrees Celsius). The most severe type of heat disease is heatstroke, commonly referred to as sunstroke. Heatstroke can result in unconsciousness, organ failure, brain damage and even death. Heatstroke can happen to anyone. However, because to potential limitations in their bodies' capacity to adequately regulate temperature, newborns and the elderly are particularly at risk. In order to protect elderly and other vulnerable persons from the heat levels that are anticipated over the next ten years, simpler solutions can be quite effective. Heatstroke can also happen to persons who work physically demanding jobs in hot areas, such as athletes, soldiers, and people in other professions. When your body is unable to cool itself down, heatstroke happens. Your brain's hypothalamus, which regulates a number of internal processes, governs your body's core temperature. Usually, it sets your thermostat to 98.6 degrees Fahrenheit (37 degrees Celsius). However, if your body absorbs more heat than it expels, the set-point for your internal temperature is exceeded. Heatstroke needs immediate first aid to lower the body temperature as quickly as possible. It's most common in urban areas during periods of very hot weather. Some predictions state that as global warming progresses, heat-related mortality will dramatically increase, yet current evidence is generally reassuring. The populations of hot places have adapted to their hotter summers through physiological or other methods. As the current hot weather has served as a reminder, climatic warming is not constant and is occasionally interrupted by unpredictability. These can suddenly expose populations to temperatures they have never experienced before and are unprepared for, like in the case of the recent heat wave. Although oral fluids and occasionally intravenous saline and dextrose must be administered to patients with heat stroke, preventative measures are by far the most crucial.

The virus normally attacks the lungs in the human body and causes pneumonia in severe cases. Subsequently, it decreases the oxygen level instantly. Because this virus has no cure thus far, the only solution before a vaccine is to prevent the spread of the virus. Therefore, tests and traces are the only solutions so far. Normally, the polymerase chain reaction (PCR) test is widely used in medical science for this. However, because the number of cases is increasing rapidly, it has become nearly impossible to perform many tests through PCR. PCR testing is time-consuming and costly. Therefore, alternative testing is required so that infected people can be identified quickly and quarantined or isolated. To date, some deep learning approaches have been used to identify viruses. However, the results of these deep learning techniques are not sufficient to deal with a medical-related diagnosis system.

COVID-Net, a deep CNN architecture built from chest X-ray (CXR) images for the detection of COVID-19, was introduced in [6]. A research [7] was conducted to classify CXR images into three groups: a transfer learning-based CNN model was used for COVID, non-COVID, and regular pneumonia. The authors reported that the CNN-based computer aided diagnosis (CAD) method yielded an overall precision of 94.5%. In [8], a model based on the auxiliary classifier generative adversarial network, called CovidGAN, was created. They added synthetic images created by CovidGAN. The accuracy was increased to 95%. In [9], to minimise complexity and increase memory efficiency, the authors used iterativepruning. Combining modality-specific information transfer, iterative model pruning, and ensemble learning, they realised an enhanced prediction. In [10], the goal is to develop an automated deep transfer learning-based technique for detecting COVID-19 infection using the extreme version of the Inception model, with 95% accuracy in InceptionV3. The authors of [11] constructed DRE-Net and used ResNet50 as a pretrain model, which is based on MobileNetV2. To extract image details, they used feature pyramid networks. This study was based on image data augmentation. The authors of [12] used AlexNet and GoogLeNet, and two separate DCNNs were used to classify the images as having pulmonary manifestations: tuberculosis or healthy. In [13], five different types of pretrained models were used for the detection of coronavirus-infected patients using chest X-ray radiographs: InceptionV3, Inception-ResNetV2, ResNet152, ResNet50, and ResNet101. In [14], they proposed a classification model that was analysed by VGG16 with an accuracy of 95.9%, whereas in [15], the authors used MobileNetV2 for different datasets along with VGG19, where 97.40% accuracy was obtained in MobileNetV2. Further, the fine-tuned ResNet50 has 92% accuracy in the study by [16].

Most studies obtained an accuracy of approximately 90%. Conversely, the present paper study used some pretrained models. That is, ImageNetV2 with customization yielded 98% accuracy and validation accuracy of 97%; VGG16, accuracy of 98% and validation accuracy of 98%; ResNet50, accuracy of 88% and validation accuracy of 91%; and InceptionV3, accuracy of 98% and validation accuracy of 99%. The designed custom CNN model obtained 97% accuracy and 97% validation accuracy. Clearly, the accuracy percentage of the models used in this study is higher than those of previous studies, making the models in the current study more reliable. Their robustness has been verified through multiple model comparisons, and the scheme can be drawn through study analysis.

This paper describes a deep learning approach for identifying SARS-CoV-2-infected patients. In the classification, feature extraction in the CNN model can be achieved with high performance. Filter-based feature extraction is used in the CNN model, which can be effective for classification. CNNs can classify images with complex identities. A large number of weight parameters can be reduced using the CNN architecture. Considering these facts, this paper proposes different CNN architectures to detect COVID-19 [17], specifically using CT scan images. In this study, CXR images were used as a sample dataset because X-ray equipment is low cost and time-efficient, as well as small and available in almost every clinic. Therefore, fewer developing countries can benefit from this research. This system will help detect coronavirus from CXR images within the shortest possible time. One of the most common radiological tests is chest radiography. CXR analysis involves the detection and localization of thoracic illnesses. This will reduce the pressure on PCR test, which is costly and time-consuming. False negatives are a common issue in PCR test results, which is not helpful for the current situation. If we can develop a model with very high accuracy, false result problems can be resolved. If this test could be introduced, more people could be tested in a short time, and thus the spread could be decreased significantly.

The remainder of the paper is organised as follows. The materials and procedures are covered in Section 2. Section 3 presents the findings and analysis. Finally, in Section 4, the conclusion is presented.

2 Methods and Materials

The dataset was obtained from the open source Kaggle and GitHub and then merged to prepare a suitable dataset. The dataset is a tabular one consisting of columns on Daily Ingested Water (L), Time of year (month), Cardiovascular disease history, Dehydration, Heat Index (HI), Diastolic BP, Environmental temperature (C), Sickle Cell Trait (SCT), Systolic BP, Weight (kg), Patient temperature, Rectal temperature (deg C), Relative Humidity, Exposure to sun, BMI, Exertional (1) vs classic (0), Barometric Pressure, Heart / Pulse rate (b/min), Age, Sweating, Skin color (flushed/normal=1, pale=0.5, cyatonic=0), Strenuous exercise, Nationality, Sex, Hot/dry skin, Time of day, Heat stroke.

In this study, xAI is also used so that the approval and acceptance of the designed model can be explained.

2.1 Materials and Tools

Python is the ideal programming language for data analysis. Deep learning-based challenges are particularly effective with Python programming because of Python's large library access. To utilise a personal GPU for dataset preprocessing, Anaconda Navigator and Jupyter Notebook were used, as well as Google Colab, to handle large datasets and model training online.They were also used to save all data, code, and work so that it can be retrieved from any GPU using GitHub. Because GitHub has a tracking system for teamwork and code management, it is also suitable for teamwork.

2.2 Dataset Description

The dataset is a tabular one of 609 different cases. It consists of 26 different colums, each contributing important information on facts related to heat stroke. The 26 different classes are as follows: Daily Ingested Water (L), Time of year (month), Cardiovascular disease history, Dehydration, Heat Index (HI), Diastolic BP, Environmental temperature (C), Sickle Cell Trait (SCT), Systolic BP, Weight (kg), Patient temperature, Rectal temperature (deg C), Relative Humidity, Exposure to sun, BMI, Exertional (1) vs classic (0), Barometric Pressure, Heart / Pulse rate (b/min), Age, Sweating, Skin color (flushed/normal=1, pale=0.5,

cyatonic=0), Strenuous exercise, Nationality, Sex, Hot/dry skin, Time of day, Heat stroke.There were 500 cases without heatstroke and 109 cases with heatstroke. These classes were divided into two subclasses. One of them is a training set, and the other is a validation set.

Relative Humidity	Exposure to sun	BMI	Exertional (1) vs classic (0)	Barometric Pressure	Heart / Pulse rate (b/min)	Age	Sweating	Skin color (flushed/normal=1, pale=0.5, cyatonic=0)	Strenuous exercise	Nationality	Sex	Hot/dry skin	Time of day	Heat stroke
0.4	1	24	1	29.97	166	38	0	0.021013998	0.5	1	1	0	10.55062835	1
0.1	0	19.62460268	1	29.97	68	50	1	0.045986849	0	1	0	0	10.61366857	1
0.1	0	21.1240585	1	29.97	96	64	0	0.031295204	0	1	0	0	14.41961465	1
0.1	0	20.75291528	1	29.97	70	19	0	0.052653505	0	1	0	0	9.467315103	1
0.1	0	22.04836437	1	29.97	88	21	1	0.076099021	0	1	0	0	12.46031495	1
0.1	0	18.70468865	1	29.97	88	52	0	0.034125273	0	1	0	0	13.97469216	1
0.1	0	21.54601041	1	29.97	76	45	0	0.027278991	0	1	0	0	11.90626311	1
0.1	0	20.88450016	1	29.97	85	23	1	0.006342217	0	1	1	0	9.206840232	1
0.1	1	22.49814156	1	29.97	110.69734	27	1	0.053541231	1	1	1	0	10.97217595	1
0.236666667	0.5	21.08117859	1	29.97	168	12	1	0.001781453	1	1	1	0	17	1
0.1	0	21.68749886	0	29.97	164.5554027	78.4	1	0.030164443	0	1	0	0	14.65705938	1
0.1	0	20.96022835	0	29.97	143.9053592	78.4	1	0.040385256	0	1	0	0	12.48713595	1
0.1	0	22.92546476	0	29.97	97.64676521	78.4	1	0.058054781	0	1	0	0	16.1924756	1
0.1	0	20.00075994	0	29.97	116.6741022	78.4	0	0.016502442	0	1	0	0	13.05444807	1
0.1	0	18.92977419	0	29.97	177.306114	78.4	0	0.074951105	0	1	0	0	12.84703946	1
0.1	0	18.68834387	0	29.97	152.9039796	78.4	0	0.082545681	0	1	0	0	12.96063096	1
0.1	0	21.7334487	0	29.97	76.8766746	78.4	0	0.076279005	0	1	0	0	10.41769185	1
0.43	0	19.40497834	0	29.97	144	67	0	0.067956018	0	1	1	0	15.19835015	1
0.43	0	19.29778868	0	29.97	108	25	0	0.03320121	0	1	0	0	11.76101994	1
0.43	0	19.30664297	0	29.97	120	64	0	0.017964078	0	1	1	0	16.95601056	1
0.43	0	21.83052459	0	29.97	144	60	0	0	0	1	1	0	16.58843296	1
0.473333333	0	22.21890478	0	29.97	186	43	0	1	0	1	1	0	15.29497215	1
0.473333333	0	22.73124832	0	29.97	160	62	0	1	0	1	1	0	16.76249468	1
0.473333333	0	21.09118155	0	29.97	96.47480841	64	0	0	0	1	0	0	12.33076816	1
0.473333333	0	20.12348066	0	29.97	140	49	0	1	0	1	1	0	12.77460469	1
0.473333333	0	19.29757755	0	29.97	104	50	0	0.07429789	0	1	0	0	10.4434076	1
0.473333333	0	19.03771995	0	29.97	110	65	0	1	0	1	1	0	13.18214731	1
0.416666667	0	20.35693335	0	29.97	160	39	0	1	0	1	1	0	16.31238697	1
0.416666667	0	20.59696703	0	29.97	90	67	0	1	0	1	0	0	9.898400657	1
0.416666667	0	19.86070536	0	29.97	120	76	0	0.043739794	0	1	0	0	16.22973588	1
0.416666667	0	20.88746764	0	29.97	110.9319445	65	0	0.5	0	1	1	0	10.42920008	1
0.416666667	0	19.81656124	0	29.97	128	51	0	1	0	1	0	0	12.49025262	1
0.416666667	0	19.94088394	0	29.97	43.94986445	63	0	0.05476445	0	1	1	0	15.45392073	1
0.423333333	0	19.94958734	0	29.97	108	57	0	1	0	1	1	0	16.0383039	1
0.423333333	0	20.63685382	0	29.97	140	71	0	1	0	1	1	0	12.15816486	1
0.423333333	0	18.82918998	0	29.97	90	70	0	1	0	1	1	0	16.13257382	1

Figure 1: Dataset example of patients with heatstroke, ,

Relative Humidity	Exposure to sun	BMI	Exertional (1) vs classic (0)	Barometric Pressure	Heart / Pulse rate (b/min)	Age	Sweating	Skin color (flushed/normal=1, pale=0.5, cyatonic=0)	Strenuous exercise	Nationality	Sex	Hot/dry skin	Time of day	Heat stroke
0.196760063	0.205992183	20.18281622	0	29.97	153.5502455	22.47479303	1	0.064268633	0.667236019	1	0	0	12.51238423	0
0.074533244	0.444810993	20.45848206	0	29.97	105.4043965	35.46297772	0	0.020284241	0.634191365	1	0	0	12.33646761	0
0.093441065	0.250650421	19.31389512	0	29.97	121.2912307	48.31197108	1	0.016522153	0.166986411	0	0	0	12.15807058	0
0.245686587	0.419641812	21.31593599	0	29.97	147.7073109	19.76758374	1	0.010249419	0.754148349	0	1	0	13.08816853	0
-0.00648502	0.23019512	21.50107058	0	29.97	132.4011086	52.54834816	1	0.077776555	0.770245825	0	1	0	9.687264119	0
0.168987262	0.483962983	22.84425967	0	29.97	103.9230189	46.41642873	0	0.084594637	0.440235354	1	0	0	12.99360069	0
0.178710789	0.422321087	20.2490205	0	29.97	120.9624501	52.28943746	1	0.080010794	0.731832151	0	0	0	13.12572905	0
-0.178784919	0.164447957	20.22532358	0	29.97	99.4657306	19.38311763	1	0.001149967	0.525544954	0	1	0	16.78258257	0
0.182492197	0.276202013	22.40867269	0	29.97	130.2196832	30.821705	1	0.028856171	0.281864831	1	1	0	10.81280728	0
-0.041464728	0.305040837	20.40068297	0	29.97	83.85987736	47.36118952	1	0.084591699	0.519125534	1	0	0	9.838459803	0
0.084206693	0.417344274	21.74976958	0	29.97	106.9875603	40.76352066	1	0.038699863	0.330133078	1	0	0	10.21842603	0
0.085441875	0.271230744	22.18199583	0	29.97	182.5243928	32.5058079	0	0.023224055	0.823670557	0	1	0	9.55092725	0
0.092871612	0.217242132	21.10196212	0	29.97	143.7884143	49.49367788	1	0.053072442	0.555979308	0	0	0	16.16820273	0
0.127053625	0.328262124	21.77234366	0	29.97	108.553566	22.3029397	0	0.055829098	0.670725398	0	0	0	12.71235811	0
0.097113244	0.410444682	21.11555545	0	29.97	103.2811001	33.37493679	0	0.062155638	0.72362805	1	0	0	10.76846014	0
0.070868683	0.218158649	19.69951326	0	29.97	99.09068638	45.50114558	0	0.007614459	0.698294136	1	0	0	15.38576318	0
0.261249072	0.355740049	18.82464139	0	29.97	140.9059835	25.1328849	0	0.055390277	0.775143744	0	0	0	13.19226682	0
0.306108603	0.302892765	22.82222897	0	29.97	122.304889	45.50663526	1	0.035500955	0.288691174	1	1	0	11.27131752	0
0.03462032	0.226550282	22.2638641	0	29.97	97.05071428	45.13183806	1	0.065214617	0.464121351	0	1	0	11.03985965	0
0.215884025	0.363684235	19.72892164	0	29.97	148.2028216	37.30697183	0	0.018753468	0.566042638	0	0	0	12.55702984	0
0.165354442	0.351653001	20.797795	0	29.97	110.5248323	49.03599805	1	0.034210978	0.840884067	0	1	0	9.060058794	0
0.048403075	0.279508239	18.61983114	0	29.97	115.6123419	19.29914429	0	0.054053004	0.042750388	1	0	0	15.8080943	0
0.106444664	0.33367747	19.75627364	0	29.97	130.8467307	41.13610201	0	0.010280766	0.363894455	1	0	0	11.30773352	0
0.143977782	0.335233044	22.23660994	0	29.97	128.0076937	51.04989169	0	0.006141147	0.885473362	1	0	0	13.86816811	0
0.025395984	0.286913527	21.89637254	0	29.97	142.8901056	42.77873729	1	0.034727168	0.511070079	0	1	0	12.38168581	0
0.016856636	0.467425355	20.29681347	0	29.97	130.426776	36.52300731	1	0.04165723	0.567497795	1	0	0	10.89270973	0
0.146917117	0.389687438	20.78764931	0	29.97	118.8783575	45.93340949	1	0.078589705	0.893489879	1	0	0	15.2031342	0
0.126499344	0.120655489	20.12553305	0	29.97	117.1147767	30.77107563	0	0.029187987	0.499731565	1	0	0	11.96138315	0
0.148886512	0.296432047	18.89976208	0	29.97	106.8207841	51.3792361	1	0.02185475	0.46148248	1	0	0	12.53399518	0
0.212117847	0.081062253	22.69333412	0	29.97	120.6022632	33.52474146	1	0.021765995	0.041242358	1	0	0	11.9741764	0
0.288719153	0.234954973	19.62678654	0	29.97	90.72928387	43.69312188	0	0.013720417	0.817460253	0	1	0	14.59449628	0
0.253558004	0.415630697	21.52743823	0	29.97	116.8298858	35.84395758	1	0.031535009	0.288373556	0	1	0	13.44643284	0
0.138062679	0.480293841	20.58447808	0	29.97	103.9319057	28.34146668	1	0.02650882	0.658966569	0	0	0	14.56960185	0
0.035768912	0.344501248	21.48517278	0	29.97	113.26981	18.61252491	1	0.060540711	0.480055099	0	0	0	12.95341622	0
0.221421514	0.607292586	21.95629649	0	29.97	103.9664298	29.75970864	1	0.059627471	0.686152861	0	0	0	10.90829578	0
0.051509859	0.351481456	22.2940252	0	29.97	117.0961646	28.81627201	1	0.061819036	0.244897588	0	0	0	14.61961354	0

Figure 2: Dataset example of patients without heatstroke

Fig. 1 shows a screenshot of the table consisting of people who had heatstrokes, and Fig. 2 shows a normal unaffected people.

2.3 Block Diagram

In the block diagram of Fig. 3, the input is given as a table, which has two subsections: heatstroke patients and normal patients.

In the block diagram, the overall system is provided in the simplest manner. The decision part of this system is crucial and plays a vital role in this study. The decision is mainly based on the model, which is trained with a large amount of data that is extracted from CXR images.

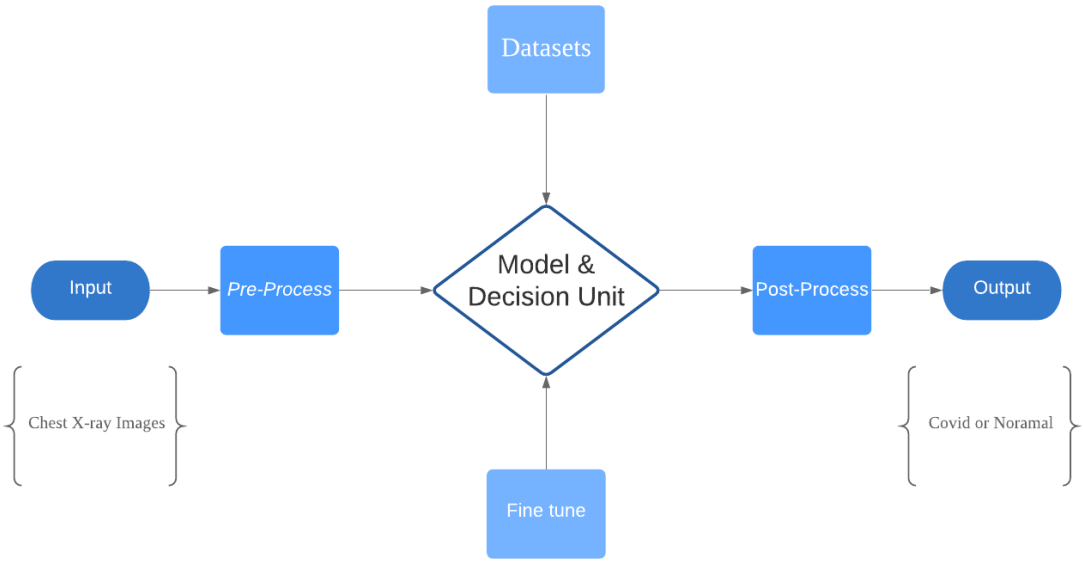

Figure 3: Block diagram of the system

2.4 System Architecture

The system architecture is an overview of the entire system. In this architecture, the input is a table, and the output is a prediction of the table. In this case, it will predict whether the data is likely to be affected by heatstroke. The input shape is 26 × 609. In the first two layers of the designed architecture, an ANN consisting of two dense layers is used to get the predictions and the activation function used is ReLU and Sigmoid. Fig. 4 shows a bird's view of the architecture.

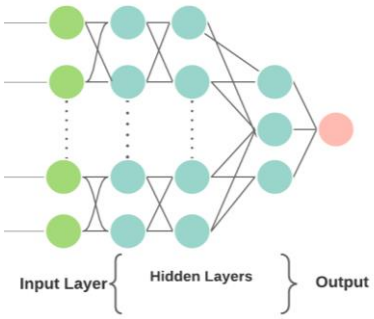

Figure 4: System architecture

2.4.1 Convolutional Layer

The convolutional layer is the basic layer of CNN. This is accountable for determining the design characteristics. The input picture is passed through a filter in this layer. The function map is obtained from the output of the same filters by convolution operation.

The multiplication of sets of weights with the input is performed by a convolution operation. A filter consists of a two-dimensional collection of weights multiplied by an array of input data. A dot product is a type of multiplication that is applied between a filter-sized patch of the input and the filter, which results in a single value. This product is applied between the filter-sized patch of the input and the filter. The filter is smaller than the input, and the same filter is used to multiply the input from different points. The filter is

designed as a special technique to identify specific types of features as it systematically covers the entire image.

Assume that the NN input is $V \in R^{A\times B}$, where A denotes the number of features that indicate an input frequency band and B denotes the total number of input frequency bands. The size of the filter bank function vector is represented by B in the case of filter bank features. Assume that v = [v1 v2... vB], where vBdenotes the function vector for band b. The activations of the convolution layer can be calculated as

$$h_{j,k} = \theta\left(\sum_{b=1}^{s} w_{b,j}^{T} v_{b+k-1} + a_j\right), \qquad (1)$$

where $h_{j,k}$ is the j^{th} feature map's convolution layer output of the convolution layer band of k^{th}, s indicates the filter scale, $w_{b,j}$ indicates the weight vector for the j^{th} filter's bth band, a_j is the j^{th} feature map's bias, and (x) represents the activation function [19].

2.4.2 Pooling Layer

The pooling layer summarizes the presence of features by facilitating the downsampling of features. It is normally applied after a convolution layer and has some spatial invariance. Two popular pooling methods, average pooling and max pooling, summarize the average presence of a function and the most activated presence of a function [20].

In fact, the pooling layer deletes the unnecessary features from the images and makes the images literate. In average pooling, the layer averages the value of its current view every time. When using maxpooling, the layer selects the maximum value from the filter's current view each time. Using the matrix size specified in each feature map, the max-pooling technique selects only the maximum value, resulting in reduced output neurons. Thus, the size of the image becomes very small, but the scenario remains the same. A pooling layer is important for reducing the number of feature maps and network parameters, and a dropout layer is used to prevent overfitting.

The activation of max pooling can be calculated as follows:

$$p_{j,m} = max_{k=1}^{r}\left(h_{j,(m-1)(n+k)}\right), \qquad (2)$$

where $p_{j,m}$ is the performance of the pooling layer of the jth function map and the mth pooling layer band, n is the subsampling factor, r is the pooling scale which is the number of bands to be pooled together, and n is the subsampling factor.

2.4.3 Flatten Layer

The flattened layer is used to convert data from the matrix into a one-dimensional array for use in the fully connected layer and to create a single one-dimensional feature that is both long and narrow. Flattening vectors are an option. Finally, it connects the single vector to the final classification model, which is also known as a fully connected layer [21]. All pixel data is given in one and connected with fully connected layers. Flattening and fully connected layers are the last few steps of CNN. It is prepared for the next fully linked layer of picture categorization by converting it into a one-dimensional array.

2.4.4 Fully Connected Layer

CNNs rely mostly on fully connected layers, which have proven to be quiteuseful in computer vision image recognition and classification. Convolution and pooling are the starting levels of the CNN process, which breaks down the image into attributes and analyses them separately [22].

In a fully connected layer, each input is connected to all neurons, and the inputs are flattened. The ReLU activation function is commonly used as a fully connected layer. The softmax activation function was used to predict the output images in the last layer of the fully connected layer. The convolutional neural network architecture uses a fully connected layer. These are the last few layers and important layers of the convolutional neural network.

3 Result and Analysis

After training the model with the train generator, validation generator, step per epoch=16, and 100 epochs, our model provided 98.56% accuracy and 3.96% loss in the 100th epoch of our model. In the first few epochs, the accuracy of the training was quite low, starting at 59.14%, and after the 100th epoch, it changed to 98%.

	precision	recall	f1-score	support
0	0.97	1.00	0.99	100
1	1.00	0.86	0.93	22
accuracy			0.98	122
macro avg	0.99	0.93	0.96	122
weighted avg	0.98	0.98	0.97	122

Table 1: Histories of the accuracy and loss of the model

3.1 Model Explainability

The premise of this paper is to mainly implement xAI. Attached are some of those graphs to show how xAI opens new doors to be used in the medical community.

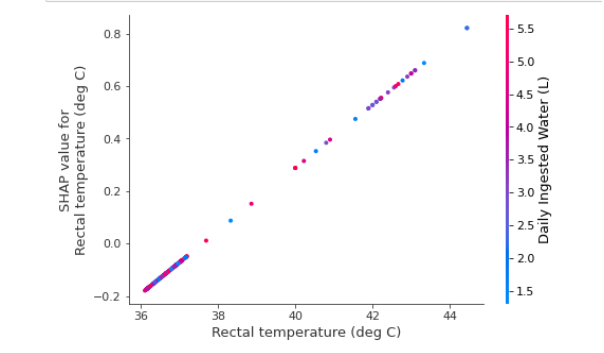

(a)

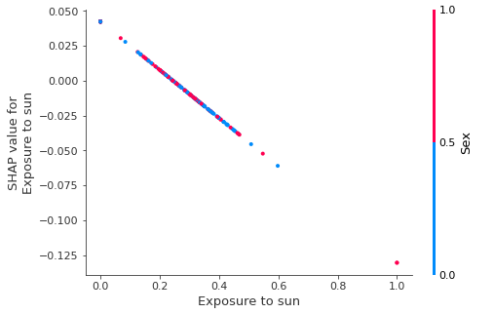

(b)

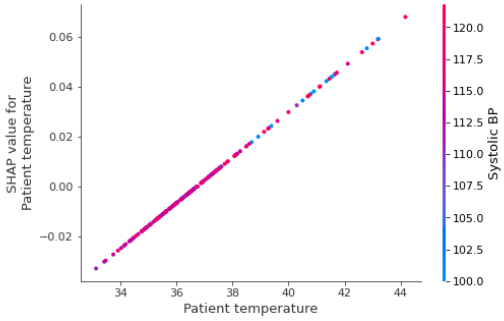

(c)

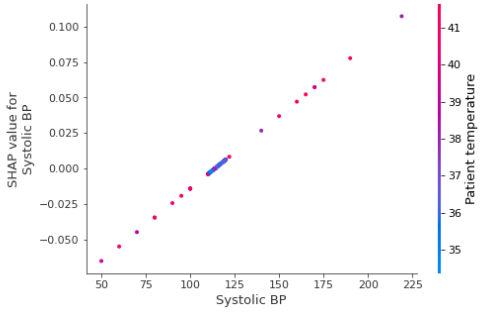

(d)

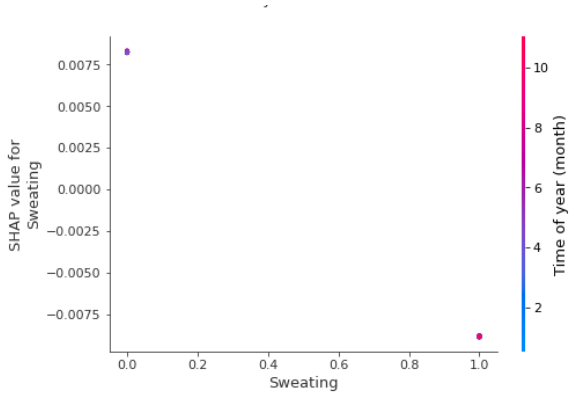

(e)

Figure 6: (a) Rectal temperature (deg C) vs shap_values and (b) Exposure to sun vs shap_values (c) Patient temperature vs shap_values, (d) Systolic BP vs shap_values, (e) Sweating vs shap_values

3.2

Confusion Matrix

The systems plotted a confusion matrix, with columns representing real values and rows representing predicted values. In a classification model, the summary of the prediction results is known as the confusion matrix. In the confusion matrix, correct and incorrect predictions are summed and split down by class, and the forn $\times n$ matrices FP, FN, TP, and TN are calculated using Eqs. (3), (4), (5), and (6) [28].

$$TP_i = a_{ii} \tag{3}$$

$$FP_i = \sum_{j=1,j\neq i}^{n} a_{ji} \tag{4}$$

$$FN_i = \sum_{j=1,j\neq i}^{n} a_{ij} \tag{5}$$

$$TN_i = \sum_{j=1,j\neq i}^{n} \sum_{k=1,k\neq i}^{n} a_{jk} \tag{6}$$

Fig. 11 shows the confusion matrix.

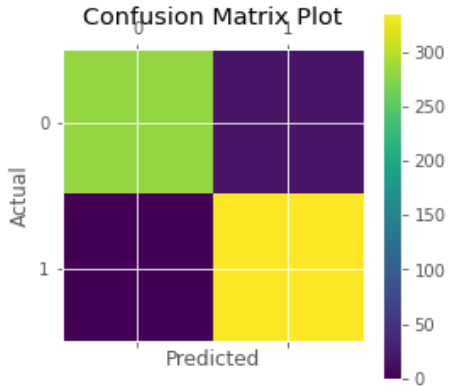

Figure 11: Confusion matrix

Three terms are important in error analysis. These are predictions, data, and features. Prediction-based

error analysis can be performed using a confusion matrix, where it can be visualised by the percentage of true positives, true negatives, false positives, and false negatives. Data size and nature are also important for error analysis. Splitting the data accordingly for making trains and tests is also considerable for error analysis because the training and test sets may affect the results on a large scale. Features play a vital role in error analysis. Feature engineering and regularisation were also performed to reduce errors.

3.4 Model Evaluation

The performance analysis of the models is evaluated based on accuracy, precision, recall, and F1-score. The performance of the proposed model was assessed using the terms true positive (TP), false positive (FP), true negative (TN), and false negative (FN). The rate of properly detecting the affected photographs from all images is referred to as recall, also called sensitivity. Precision is the opposite of recall. The F1-score is a combined measure of precision and recall, which shows how often the predicted value is accurate. It is also known as the harmonic mean of p and r in mathematics. These equations are given below.

Matrixes can be used to evaluate a system's performance, and after the development of the model, its performance, which performance. Accuracy is a measure of how well a model or system works (i.e., the number of times the model correctly predicts the actual outcome) should be calculated. The mathematical formulas for determining the accuracy are expressed in Eqs. 7 and 8 [29].

$$accuracy = \frac{TP+TN}{TP+TN+FP+FN} \tag{7}$$

$$accuracy = \frac{correctpredictions}{totalnumberofexample}. \tag{8}$$

The rate of successfully detecting the real value from a set of all values is recognised as recall, also called sensitivity. Recall can be determined using the expression in Eq. (9) [30].

$$re - call = \frac{TP}{TP+FN}. \tag{9}$$

The number of correct identifications is referred to as precision. The number of times the model's positive forecast was right can be calculated, and this is more related to the model's positive identification, using the following mathematical formula Eq. (10).

$$precision = \frac{TP}{TP+FP}. \tag{10}$$

For both recall and precision, a single matrix can be used to summarize the classifier's performance, and the F1-score is a single matrix that characterizes precision and recall. It is also known as a harmonic means of precision and recall in other mathematical words.The F1-score is calculated using Eq. (11).

$$f1 - score = \frac{2pr}{p+r}. \tag{11}$$

In Eqs. 3 and 4, TP stands for true positive, FP for false positive, and FN for false negative. The letters p and r in Eq. 10 represent precision and recall, respectively. Model evaluation of precision, recall, and F1-score of our custom CNN models, MobileNetV2, VGG16, and InceptionV3 is given in Table 2. It shows that InceptionV3 and MobileNetV2 have higher precision, recall, and F1-score values than the other models. InceptionV3 performs exceptionally well among other models, and its accuracy also yielded higher results, which are shown in Table 1.

4 Conclusion

In this study, ANN and xAI models were presented, namely, a full custom ANN. The models used in this study obtained almost the same accuracy. The dataset contains 609 cases of which 109 were affected by heatstroke. The accuracy of the model was 98%, whereas the precision recall and f2 scores are 97%, 100% and 99%. Further work will be performed on a larger dataset and with other pretrained models.. Thus, it could be an efficient method for detecting COVID-19 patients. To test and trace the virus, this method is quick and has no risk of standing in a queue to test COVID-19 and spreading the virus.

This innovation will greatly change the medical sector. Using this technique, heat stroke patients can quickly identify, which may contribute to addressing the current pandemic situation. Chest radiography is comparably safer for obtaining a sample than from the nose of a patient. In the future, this type of technique will help human beings. Several deep learning techniques can be used to optimise the parameters to create a robust model which can help mankind. The metaheuristic-based deep heat stroke model could also be a good technique to be explored in the future [31]. Some more transfer learning-based models can be added in further development to compare the accuracy and optimisation of parameters [32], as well as a large dataset of normal and heat stroke patients. The results can be observed by changing the ratio of training and testing data, and further comparative analysis can be performed. Analysing risk and survival would be an effective study for further development [33]. In the current scenario, as the volume of patients is quite high, deep learning-based COVID-19 detection systems can be helpful. For more accurate results, different types of CNN architecture were introduced. This technology will inspire future generations to address this unwanted situation.

Data Availability Statement: The data used to support the findings of this study are freely available at https://www.kaggle.com/datasets/tahiatazin1510997643/heat-stroke?fbclid=IwAR2COdQGwk3oIVZII8i23_HdcI9j3mfNyaXrkwMU6374iKdIbu-qtkYk9Es

Funding Statement:

Conflicts of Interest: The authors would like to confirm there are no conflicts of interest regarding the study.

References

[1] K. Thiagarajan, “Why is India having a covid-19 surge?, ”*BMJ*, pp.1-3,202. Available: https://www.bmj.com/content/bmj/373/bmj.n1124.full.pdf

[2] Rafferty, J. P. (Invalid Date). India-Pakistan heat wave of 2015. Encyclopedia Britannica. https://www.britannica.com/event/India-Pakistan-heat-wave-of-2015"WHO coronavirus (COVID-19) dashboard", *WHO*, 2021. Available: https://covid19.who.int/

[3] Koppe, Christina, Kovats, Sari, Jendritzky, Gerd & Menne, Bettina. (2004). Heat-waves: risks and responses. World Health Organization. Regional Office for Europe. https://apps.who.int/iris/handle/10665/107552

[4] R. Sethi, M. Mehrotra and D.Sethi, "Deep Learning based Diagnosis Recommendation for COVID-19 using Chest X-Rays Images," *2020 Second International Conference on Inventive Research in Computing Applications (ICIRCA)*, pp. 1-4, 2020. doi: 10.1109/ICIRCA48905.2020.9183278.

[5] L. Wang, Z. Lin and A. Wong, "COVID-Net: a tailored deep convolutional neural network design for detection of COVID-19 cases from chest x-ray images," *Scientific Reports*, vol. 10, no. 1, pp. 1-4, 2020. Available: 10.1038/s41598-020-76550-z

[6] M. Heidary, S. Mirniaharikandehei and A. Khuzani, “Improving the performance of CNN to predict the likelihood of COVID-19 using chest X-ray images with preprocessing algorithms,” *International Journal of Medical Informatics*, vol. 144, no. 2, pp. 1-3, 2020.

[7] A. Waheed, M. Goyal, D. Gupta, A. Khanna, F. Al-Turjman and P. R. Pinheiro, "CovidGAN: Data augmentation using auxiliary classifier GAN for improved covid-19 detection," *IEEE Access*, vol. 8, pp. 91916-91923, 2020.

[8] S. Rajaraman, J. Siegelman, P. Alderson, L. Folio, L. Folio and S. Antani, "Iteratively Pruned Deep Learning Ensembles for COVID-19 Detection in Chest X-Rays", *IEEE Access*, vol. 8, pp. 115041-115050, 2020. Available: 10.1109/access.2020.3003810.

[9] N. N. Das, N. Kumar, M. Kaur, V. Kumar and D. Singh, "Automated deep transfer learning-based approach for detection of COVID-19 infection in chest x-rays," *IRBM*, pp.2-4, 2020.

[10] S. Ying *et al.*,"Deep learning enables accurate diagnosis of novel coronavirus (COVID-19) with CT images," *IEEE/ACM Transactions on Computational Biology and Bioinformatics*, pp. 1-2, 2020.Available: 10.1101/2020.02.23.20026930

[11] P. Lakhani and B. Sundaram, "Deep learning at chest radiography: automated classification of pulmonary tuberculosis by using Convolutional neural networks," *Radiology*, vol. 284, no. 2, pp. 574-582, 2017. Available: 10.1148/radiol.2017162326.

[12] A. Narin, C. Kaya and Z. Pamuk, "Automatic detection of coronavirus disease (COVID-19) using X-ray images and deep convolutional neural networks," *Pattern Analysis and Applications*, 2021.Available: 10.1007/s10044-021-00984-y

[13] A. Shelke et al., "Chest X-ray Classification Using Deep Learning for Automated COVID-19 Screening", *SN Computer Science*, vol. 2, no. 4, 2021. Available: 10.1007/s42979-021-00695-5.

[14] I. Apostolopoulos and T. Mpesiana, "Covid-19: automatic detection from X-ray images utilizing transfer learning with convolutional neural networks," *Physical and Engineering Sciences in Medicine*, vol. 43, no. 2, pp. 635-640, 2020. Available: 10.1007/s13246-020-00865-4

[15] A. Ismael and A. Şengür, "Deep learning approaches for COVID-19 detection based on chest X-ray images," *Expert Systems with Applications*, vol. 164, pp. 114054, 2021. Available: 10.1016/j.eswa.2020.114054

[16] Q. Li, W. Cai, X. Wang, Y. Zhou, D. D. Feng and M. Chen, "Medical image classification with convolutional neural network," *13th International Conference on Control Automation Robotics & Vision (ICARCV)*, pp. 844-848, 2014.

[17] T. Rahaman, “COVID-19 radiography database,” *Kaggle*, 2020. [Online]. Available: https://www.kaggle.com/tawsifurrahman/covid19-radiography-database

[18] O. A. Hamid, L. Deng, D. Yu, "Exploring convolutional neural network structures and optimization techniques for speech recognition,”*ISCA*,Vol. 11, pp. 73-5, 2013. Available: https://www.microsoft.com/en-us/research/publication/exploring-convolutional-neural-network-structures-and-optimization-techniques-for-speech-recognition/

[19] J. Brownlee, "A gentle introduction to pooling layers for convolutional neural networks", *Machine Learning Mastery*, 2021. Available: https://machinelearningmastery.com/pooling-layers-for-convolutional-neural-networks/

[20] J. Jeong, "The most intuitive and easiest guide for CNN," *Medium*, 2021. Available: https://towardsdatascience.com/the-most-intuitive-and-easiest-guide-for-convolutional-neural-network-3607be47480

[21] S. Saha, "A comprehensive guide to convolutional neural networks—the ELI5 way," *Medium*, 2021. Available: https://towardsdatascience.com/a-comprehensive-guide-to-convolutional-neural-networks-the-eli5-way-3bd2b1164a53

[22] I. Apostolopoulos and T. Mpesiana, "Covid-19: automatic detection from X-ray images utilizing transfer learning with convolutional neural networks," *Physical and Engineering Sciences in Medicine*, vol. 43, no. 2, pp. 635-640, 2020. [Online]. Available: 10.1007/s13246-020-00865-4

[23] M. Sandler, A. Howard, M. Zhu, A. Zhmoginov and C. L. Chieh, “MobileNetV2: inverted residuals and linear bottlenecks,” *IEEE Conference on Computer Vision and Pattern Recognition (CVPR),* pp. 4510-4520, 2018.

[24] A. G. Howard, M. Zhu, B. Chen, D. Kalenichenko, W. Wang *et al.,*“MobileNets: efficient convolutional neural networks for mobile vision applications,”*arXiv*,pp.1-7, 2017. Available: https://arxiv.org/abs/1704.04861

[25] C. Sitaula, and M. B. Hossain, “Attention-based VGG-16 model for COVID-19 chest X-ray image classification,” *Springer Science+Business Media, LLC, part of Springer Nature,* vol. 51, no.5, pp. 2850-2863, 2020.

[26] K. Simonyanand A. Zisserman, “Very deep convolutional networks for large-scale image recognition,” *arXiv* pp.1-8, 2015. Available: https://arxiv.org/abs/1409.1556v4

[27] M. S. Junayed et al., "AcneNet - A Deep CNN Based Classification Approach for Acne Classes," *2019 12th International Conference on Information & Communication Technology and System (ICTS)*, 2019, pp. 203-208.

[28] P. D. Ailab, “Evaluation: from precision, recall and F-measure to ROC, informedness, markedness& correlation,” *Machine Learning Technologies*,vol.2. pp. 37-63, 2011..Available: http://www.bioinfo.in/contents.php?id=51

[29] C. Goutte and E. Gaussier, "A probabilistic interpretation of precision, recall and f-score, with implication for evaluation," *Lecture Notes in Computer Science*, pp. 345-359, 2005. Available: 10.1007/978-3-540-31865-1_25

[30] M. Kaur, V. Kumar, V. Yadav, D. Singh, N. Kumar and N. Das, "Metaheuristic-based Deep COVID-19 Screening Model from Chest X-Ray Images", *Journal of Healthcare Engineering*, vol. 2021, pp. 1-9, 2021. Available: 10.1155/2021/8829829.

[31] D. Singh, V. Kumar, V. Yadav and M. Kaur, "Deep Neural Network-Based Screening Model for COVID-19-Infected Patients Using Chest X-Ray Images", *International Journal of Pattern Recognition and Artificial Intelligence*, vol. 35, no. 03, p. 2151004, 2020. Available: 10.1142/s0218001421510046.

[32] N. Gianchandani, A. Jaiswal, D. Singh, V. Kumar and M. Kaur, "Rapid COVID-19 diagnosis using ensemble deep transfer learning models from chest radiographic images", *Journal of Ambient Intelligence and Humanized Computing*, 2020. Available: 10.1007/s12652-020-02669-6